NET-BARYON NUMBER FLUCTUATIONS*

C. Schmidt, J. Goswami, G. Nicotra, F. Ziesché

Universität Bielefeld, Fakultät für Physik, 33615 Bielefeld, Germany

P. Dimopoulos, F. Di Renzo, S. Singh, K. Zambello

Dipartimento di Scienze Matematiche, Fisiche e Informatiche
Università di Parma and INFN, Gruppo Collegato di Parma
43100 Parma, Italy

(Received January 8, 2021)

The appearance of large, non-Gaussian cumulants of the baryon number distribution is commonly discussed as a signal for the QCD critical point. We review the status of the Taylor expansion of cumulant ratios of baryon number fluctuations along the freeze-out line and also compare QCD results with the corresponding proton number fluctuations as measured by the STAR Collaboration at RHIC. To further constrain the location of a possible QCD critical point, we discuss poles of the baryon number fluctuations in the complex plane. Here, we use not only the Taylor coefficients obtained at zero chemical potential but perform also calculations of Taylor expansion coefficients of the pressure at purely imaginary chemical potentials.

DOI:10.5506/APhysPolBSupp.14.241

1. Introduction

The phase diagram of Quantum Chromodynamics (QCD) is currently investigated with large efforts by means of heavy-ion experiments at the LHC and RHIC, as well as by numerical calculations of lattice regularized QCD. While lattice calculations at vanishing chemical potential made great progress in the last decades, they are still harmed by the infamous sign problem at nonzero chemical potential. The two main methods that are currently used to infer on the QCD phase diagram at nonzero baryon chemical potential (μ_B) are indirect, they rely on Taylor expansions of observables at

* Presented at the on-line meeting *Criticality in QCD and the Hadron Resonance Gas*, Wrocław, Poland, July 29–31, 2020.

$\mu_B = 0$, or analytical continuations from simulations at imaginary chemical potential ($\mu_B = i\mu_I$). Methods that allow for a direct sampling of the oscillatory path integral at $(\mu_B) > 0$ are currently investigated, see *e.g.* [1, 2].

The two principles that are guiding our understanding of the QCD phase diagram are spontaneous chiral symmetry breaking and — linked to it — the phenomena of quark confinement. Our knowledge on the $(2 + 1)$-flavor QCD phase diagram based on recent lattice results is summarized in Fig. 1 (left). The variables assigned to the three axes are temperature (T), the

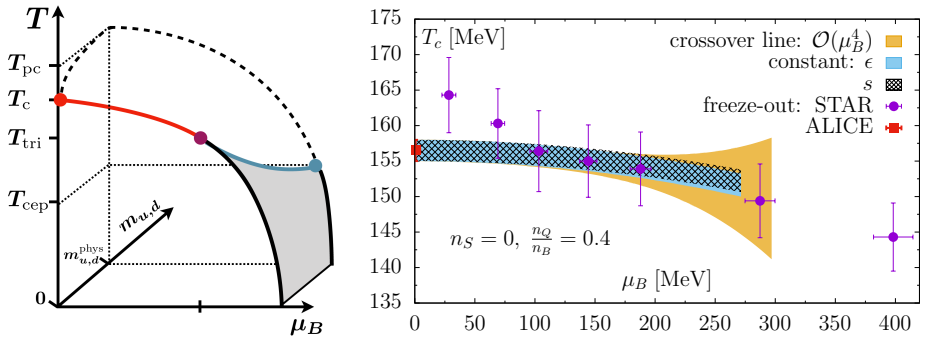

Fig. 1. (Color online) Left: Schematic picture of the QCD phase diagram. The chiral limit ($m_{u,d} = 0$) is shown in the front, whereas the physical mass case is shown in the back. Right: The chiral crossover line in $(2 + 1)$-flavor QCD, calculated with the constraints $n_S = 0$ and $n_Q = 0.4 n_B$. It is compared with the line of constant energy density $\epsilon = 0.42(6)$ GeV/fm^3 and the line of constant entropy density $s = 3.7(5)$ fm^{-3} [3] in the T–μ_B plane. Also shown are the chemical freeze-out parameters extracted from grand-canonical-ensemble-based fits to hadron yields for the ALICE [4] and the STAR [5] experiments.

baryon chemical potential (μ_B) and light quark mass ($m_{u,d}$). At low T and low μ_B, the chiral symmetry is spontaneously broken and quarks are confined into hadrons. Correspondingly, chiral symmetry is restored at high T and high μ_B, where quarks can move freely[1]. Solid dark gray/red and light gray/cyan lines indicate a continous phase transition in the universality class of the 3d–O(4) symmetric spin model, or the Z(2) symmetric Ising model, respectively. Black lines and gray surfaces indicate a discontinuous first order transition. On the temperature axis, we also indicate the pseudo-critical transition temperature at physical masses ($T_{\rm pc}$), the critical temperature in the chiral limit ($T_{\rm c}$), the temperature of the tri-critical point in the chiral limit ($T_{\rm tri}$), and the temperature of the critical (end-)point at physical quark masses ($T_{\rm cep}$). It emerges a hierarchy as

[1] For simplicity, we are neglecting here various superconducting phases at low T and high μ_B, which will not be discussed in this work.

$T_{\rm pc} > T_{\rm c} > T_{\rm tri} > T_{\rm cep}$. The first two temperatures are determined by lattice calculations as $T_{\rm pc} = 156(\pm 1.5)$ MeV [6] and $T_{\rm c} = 132^{+3}_{-6}$ MeV [7]. The variation of $T_{\rm pc}$ with μ_B, as indicated by a dashed line, has also been calculated by lattice QCD. We obtain

$$\frac{T_{\rm pc}(\mu_B)}{T_{\rm pc}(0)} = 1 - \kappa_2 \left(\frac{\mu_B}{T}\right)^2 + \mathcal{O}\left(\frac{\mu_B}{T}\right)^4 , \tag{1}$$

where $\kappa_2^B = 0.012(4)$ with an $\mathcal{O}(\mu_B^4)$ correction that vanishes within errors [6]. Similar results have been obtained recently in Ref. [8].

In Fig. 1 (right), we compare the pseudo-critical line with freeze-out temperatures and chemical potentials obtained from hadron yields measured by STAR [5] and ALICE [4]. The hadron yields have been fitted (after feed-down corrections) to the hadron resonance gas (HRG) model. In its simplest non-interacting version, this model is based on the mass spectrum of all stable particles and resonances listed in the particle data booklet, which are taken as an ideal gas in thermal equilibrium at a common temperature $T_{\rm f}$, chemical potential $\mu_{\rm f}$, and volume $V_{\rm f}$. As these parameters refer to the time in the expansion of the fireball from when on its chemical composition does not change anymore, they are called chemical freeze-out parameters. We see from Fig. 1 (right) that the freeze-out parameters agree well with the chiral crossover line obtained from lattice QCD. We note that in order to meet conditions that are found in heavy-ion collisions, we have determined our values for the electric $\mu_Q \equiv \mu_Q(\mu_B)$ and strangeness chemical potentials $\mu_S \equiv \mu_S(\mu_B)$ such that the following conditions for the net-numbers of conserved charges in the system, $\langle n_Q/n_B\rangle = 0.4$ and $\langle n_S\rangle = 0$, are fulfilled. However, the freeze-out parameters are still model based. Hence, in the following, we want to follow a procedure proposed in [9] that allows for the determination of the freeze-out parameters by a direct comparison of lattice QCD to experiment.

2. Cumulants of net-baryon number

Higher order cumulants of the net-baryon number are obtained as derivatives of the logarithm of the QCD partition functions with respect to the dimensionless parameter $\hat{\mu}_B = \mu_B/T$

$$\chi_n^B(T,\mu_B,\mu_Q,\mu_S) = \frac{1}{VT^3}\frac{\partial^n \ln Z(T,\mu_B,\mu_Q,\mu_S)}{\partial \hat{\mu}_B^n} , \tag{2}$$

where μ_Q and μ_S are the electric charge and strangeness chemical potentials. In the same way, we can also calculate derivatives with respect to μ_Q and μ_S, which we denote as χ_n^Q and χ_n^S, respectively.

Aiming at the comparison with the experimental results, we further introduce ratios of cumulants of baryon number fluctuations as

$$R^B_{nm} = \frac{\chi^B_n}{\chi^B_m} \,. \tag{3}$$

By using these ratios, the leading order dependence on the freeze-out volume (V_f) is removed. However, among other things, fluctuations of the experimentally observed freeze-out volume might still hinder a comparison to lattice QCD. The first ratio we discuss is R^B_{12}, which is shown in Fig. 2 and can be interpreted as the mean of the net-baryon number, normalized by the variance of the baryon number fluctuations. The presented HotQCD results [10] are obtained from high statistics lattice QCD calculations on $32^3 \times 8$ and $48^3 \times 12$ lattices, with $(2+1)$-flavor of highly improved staggered quarks (HISQ) at physical light- and strange-quark masses. The values in the range of $0 < \hat{\mu}_B \lesssim 1.2$ stem from a Taylor expansion of the logarithm of the partition function about $\hat{\mu}_B = 0$ to 8^{th} order in $\hat{\mu}_B$. As it is evident from the continuum estimate shown in Fig. 2 (left), the leading order of R^B_{12} is linear in μ_B. We further notice that the ratio is rather independent under the variation of temperature. Therefore, the ratio has been termed a baryometer [9].

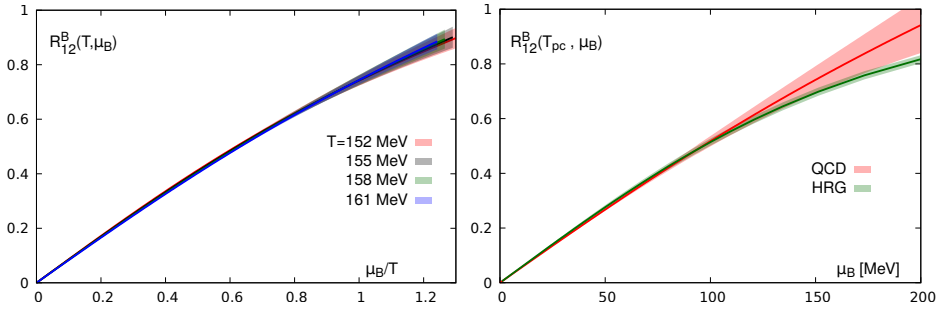

Fig. 2. Left: Continuum estimate of the cumulant ratio R^B_{12} as a function of the chemical potential, for different temperatures. Right: The same ratio along the pseudo-critical line. Shown are the QCD and HRG model results.

The same ratio is shown in Fig. 2 (right), now plotted along the pseudo-critical line as defined in Eq. (1). Here, we compare the QCD result with the corresponding calculation of a Hadron Resonance Gas (HRG). We see that the HRG model deviates from QCD only for $\mu_B \gtrsim 150$ MeV. We thus note that for small μ_B, the HRG can be used to analyze the differences between net-baryon number and net-proton number fluctuations. The latter is the quantity which is directly accessible by heavy-ion experiments. On the other hand, this also means that we do not see any indication of a diverging baryon

number fluctuation (χ_2^B) in the range where we trust our Taylor expansion, which we would expect in QCD close to a critical point. In this case, the ratio R_{12}^B would decrease and approach zero at the critical point.

As higher order cumulants are expected to diverge more rapidly when approaching a critical point, it is tempting to discuss also the ratios R_{31}^B and R_{42}^B along the pseudo-critical line, which are shown in Fig. 3 as a function of R_{12}^B [10]. Since R_{12}^B is still a monotonous function of μ_B in the plotted range, it is a measure for the baryon density and enables us to compare with the experiment in a model free way. We see that the overall agreement with the corresponding net-proton number cumulants R_{31}^P and R_{42}^P from STAR [11, 12] is very good. We conclude that a high freeze-out temperature of $T_\mathrm{f} > 155$ MeV seems to be excluded by the data. This lattice calculation is based on an 8^{th} order expansion of the logarithm of the partition function.

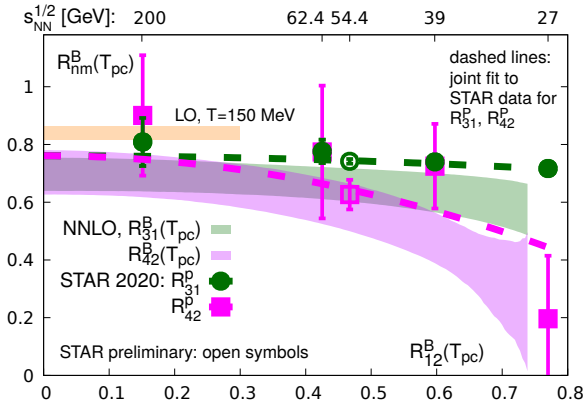

Fig. 3. The cumulant ratios (bands) R_{31}^B and R_{42}^B *versus* R_{12}^B on the pseudo-critical line, calculated from a NNLO Taylor series. Data are results on cumulant ratios of net-proton number fluctuations obtained by the STAR Collaboration [11]. Also shown are preliminary results obtained at $\sqrt{s_{NN}} = 54.4$ GeV [12]. Dashed lines show joint fits to the data.

Finally, we want to mention that the radius of convergence, which is inherent to the expansion of any thermodynamic observable, can in principle provide valuable information on the phase structure of QCD. *E.g.*, in the case of a second order phase transition, we expect the convergence radius to be limited by the critical point. A simple estimator for the radius of convergence $\hat{\rho} \equiv \mu_B^{\mathrm{crit}}/T$ is given by the ratio estimator

$$\hat{\rho} = \lim_{n\to\infty} \sqrt{(n+2)(n+1)\left|\chi_n^B/\chi_{n+2}^B\right|}\,, \tag{4}$$

more advanced estimators are also discussed [13]. Unfortunately, we have only a limited number of expansion coefficients (cumulants χ_n^B) at our dis-

posal, which makes it difficult to draw strong conclusions with given lattice data, especially, since the statistical and systematical error on higher order cumulants is drastically increasing with the order n. It is, however, interesting to note that all expansion coefficients have to be positive if the limiting singularity lies on the real axis. Hence, we can obtain an upper bound for the phase transition temperature $T_{\rm cep}$, as for $T > 140$ MeV many of the expansion coefficients turn negative [14]. This estimate is in good agreement with the statement that the temperature of the QCD critical point shall be lower than the chiral transition temperature ($T_{\rm cep} < T_{\rm c}$) as indicated in Fig. 1 (left).

3. Cumulants at imaginary chemical potential

Besides the Taylor expansion method, lattice QCD calculations can also be performed at purely imaginary chemical potential, followed by an analytic continuation of the results. The QCD partition function is symmetric under the transformation $\hat{\mu}_B \to \hat{\mu}_B + 2\pi i$. Any simulations at imaginary chemical potential are thus constrained to the interval $[-i\pi, i\pi]$ (first Roberge–Weiss sector). We further note that even/odd order cumulants on this interval are purely real/imaginary and are even/odd functions of $\mathrm{Im}[\hat{\mu}_B]$. Making use of this symmetry, we thus need to simulate only in the interval $[0, i\pi]$ and symmetrize/anti-symmetrize the data afterwards. We calculate the first four cumulants of the baryon number. Preliminary results from $24^3 \times 4$ lattices are shown in Fig. 4. We can see that the (purely imaginary) baryon number density $\mathrm{Im}[\chi_1^B]$ develops a discontinuity at $\mathrm{Im}[\hat{\mu}_B] = \pi$. The temperature where this is happening is called the Roberge–Weiss temperature ($T_{\rm RW}$), which was estimated to be $T_{\rm RW} = 201$ MeV [15] (for $N_\tau = 4$). In accordance with this discontinuity, we also observe that the second cumulant χ_2^B devel-

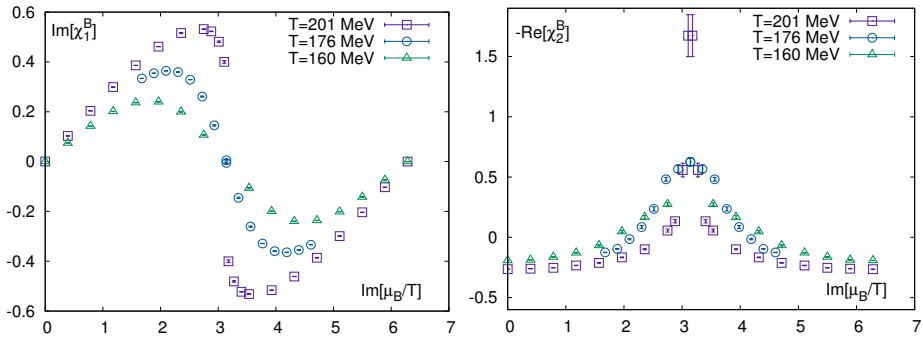

Fig. 4. Preliminary results of the first and second cumulant of the net-baryon number, χ_1^B, χ_2^B, as a function of the imaginary chemical potential for three different temperatures, obtained from calculations on $24^3 \times 4$ lattices.

ops a divergence at T_{RW}. The universal scaling of the Polyakov-loop (order parameter of the confinement transition) and chiral condensate have been investigated close to the Roberge–Weiss transition [15].

The periodic data on χ_1^B can be analyzed in terms of Fourier coefficients [16, 17], which are inherently linked to the canonical partition sums. The aim of this project is, however, to use the information of all the available cumulants to construct a precise rational function approximation, *i.e.* a $[n, m]$ Padé of χ_1^B

$$\chi_1^B \approx \mathcal{R}_n^m(\hat{\mu}_B) = \frac{P_m}{Q_n} = \frac{\sum_{i=0}^{m} a_i \, \hat{\mu}_B^i}{\sum_{j=0}^{n} b_j \, \hat{\mu}_B^j} \,. \tag{5}$$

We are currently testing several methods to determine the coefficients a_i, b_j. Among them is a direct solve method, where we directly solve a set of equations that we obtain by equating the analytic expressions for $\mathcal{R}_n^m$ as well as its first few derivatives $\partial^j \mathcal{R}_n^m / \partial \hat{\mu}_B^j$, $j = 0, 1, 2$ at each simulation point with our lattice data

$$\chi_{j+1}^B \left(\hat{\mu}_B^{(k)} \right) = \left. \frac{\partial^j \mathcal{R}_n^m \left(\hat{\mu}_B \right)}{\partial \hat{\mu}_B^j} \right|_{\hat{\mu}_B = \hat{\mu}_B^{(k)}} . \tag{6}$$

Here, $\chi_j^B(\hat{\mu}_B^{(k)})$ represent the numerical values of the cumulants at the simulation points $\hat{\mu}_B^{(k)}$, as obtained by our lattice calculations. A similar method is based on a χ^2-fit of $\mathcal{R}_n^m$ to our cumulant data. Finally, we are testing a two-step approach where in a first step, a suitable interpolation of the lattice data is chosen. In the second step, we are making use of the Remez algorithm to determine $\mathcal{R}_n^m$ until the min–max criteria are satisfied with respect to the interpolation.

Having the approximation $\mathcal{R}_n^m$ at hand, we are able to integrate the baryon density to obtain the free energy, which will also develop a cusp at T_{RW}. However, our main interest lies in the determination of the roots of the numerator P_m and denominator Q_n, which will allow us to infer information on the singularities in the complex $\hat{\mu}_B$-plane. A singularity in the complex plane is the reason for a finite radius of convergence of the Taylor series and will also indicate a true physical phase transition when it approaches the real axis in the complex $\hat{\mu}_B$-plane.

There are two models that can guide our thinking about the location of the singularities in the complex plane. At large temperatures, the thermal branch cut singularities from the Fermi–Dirac distribution of a free quark gas is expected to pinch the imaginary axis in the complex $\hat{\mu}_B$-plane. In QCD, such a behavior is expected to happen at T_{RW}. In fact, this is something we

already see, when we analyze the data shown in Fig. 4. How this thermal singularity moves in the complex plane with decreasing temperature is shown in Fig. 5 (left).

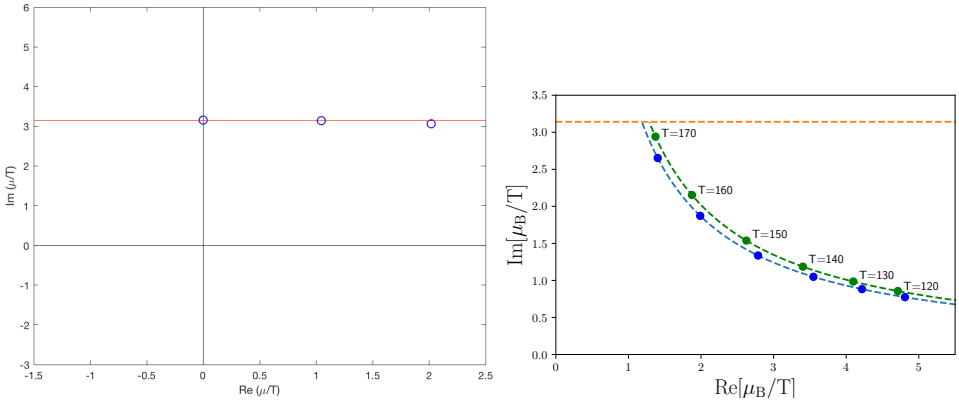

Fig. 5. (Color online) Left: Singularity in the complex plane associated with the branch cut singularity of the Fermi–Dirac distribution function of the quarks. The position of the singularity is shown for three temperatures $T = 201, 176$ and 160 MeV from left to right. The results have been obtained from calculations on $24^3 \times 4$ lattices. Right: Singularity in the complex plane associated to the pole in the scaling function $f_{\rm f}(z)$. The results are model predictions for $N_\tau = 4, 6$ (blue/lower curve, green/higher curve) based on a mapping of QCD to the universal 3d–O(2) model.

At temperatures close to the chiral transition ($T_{\rm c}$), we might be able to map our results to the universal scaling behavior connected to the chiral phase transition. The scaling function of the free energy $f_{\rm f}(z)$ will have a singularity in the complex z-plane, known as the Lee–Yang edge singularity. This singularity has been recently determined [18]. Given a mapping from QCD to the universal theory, defined by the non-universal constants $t_0, h_0, T_{\rm c}, \kappa_2^B$ [19], we can calculate the position of the singularity in the complex $\hat{\mu}_B$-plane, shown in Fig. 5 (right). Preliminary results from calculations on $36^3 \times 6$ lattices at $T = 145$ MeV seem to be in rather good agreement with this prediction. It will be very interesting but also challenging to see if the singularity will approach the real axis in the complex $\hat{\mu}_B$-plane for even smaller temperatures.

We thank all members of the HotQCD Collaboration for discussions and comments. This work is supported by the TU Deutsche Forschungsgemeinschaft (DFG, German Research Foundation) through the Collaborative Research Centre CRC-TR 211 “Strong-interaction matter under extreme con-

ditions" project number 315477589 and from the European Union's Horizon 2020 research and innovation program under the Marie Skłodowska-Curie grant agreement No. H2020-MSCAITN-2018-813942 (EuroPLEx).

REFERENCES

[1] F. Attanasio, B. Jäger, F.P. Ziegler, *Eur. Phys. J. A* **56**, 251 (2020), arXiv:2006.00476 [hep-lat].

[2] A. Alexandru *et al.*, arXiv:2007.05436 [hep-lat].

[3] A. Bazavov *et al.*, *Phys. Rev. D* **95**, 054504 (2017), arXiv:1701.04325 [hep-lat].

[4] A. Andronic *et al.*, *Nature* **561**, 321 (2018), arXiv:1710.09425 [nucl-th].

[5] L. Adamczyk *et al.*, *Phys. Rev. C* **96**, 044904 (2017), arXiv:1701.07065 [nucl-ex].

[6] A. Bazavov *et al.*, *Phys. Lett. B* **795**, 15 (2019), arXiv:1812.08235 [hep-lat].

[7] H.-T. Ding *et al.*, *Phys. Rev. Lett.* **123**, 062002 (2019), arXiv:1903.04801 [hep-lat].

[8] S. Borsanyi *et al.*, *Phys. Rev. Lett.* **125**, 052001 (2020), arXiv:2002.02821 [hep-lat].

[9] A. Bazavov *et al.*, *Phys. Rev. Lett.* **109**, 192302 (2012), arXiv:1208.1220 [hep-lat].

[10] A. Bazavov *et al.*, *Phys. Rev. D* **101**, 074502 (2020), arXiv:2001.08530 [hep-lat].

[11] J. Adam *et al.*, arXiv:2001.02852 [nucl-ex].

[12] A. Pandav, *Nucl. Phys. A* **1005**, 121936 (2021), arXiv:2003.12503 [nucl-ex].

[13] M. Giordano, A. Pásztor, *Phys. Rev. D* **99**, 114510 (2019), arXiv:1904.01974 [hep-lat].

[14] F. Karsch, *PoS* **CORFU2018**, 163 (2019), arXiv:1905.03936 [hep-lat].

[15] J. Goswami *et al.*, *PoS* **LATTICE2018**, 162 (2018), arXiv:1811.02494 [hep-lat].

[16] V. Vovchenko *et al.*, *Phys. Rev. D* **97**, 114030 (2018), arXiv:1711.01261 [hep-ph].

[17] G.A. Almási *et al.*, *hys. Rev. D* **100**, 016016 (2019), arXiv:1805.04441 [hep-ph].

[18] A. Connelly *et al.*, *hys. Rev. Lett.* **125**, 191602 (2020), arXiv:2006.12541 [cond-mat.stat-mech].

[19] HotQCD Collaboration, private communication.